DNA double-strand breaks cooperate with loss of Ink4 and Arf tumor suppressors to generate glioblastomas with frequent Met amplification

Cristel V. Camacho[1,6], **Pavlina K. Todorova**[1], **Molly C. Gillam**[1], **Nozomi Tomimatsu**[1], **Carlos R Gil del Alcazar**[1], **Mariya Ilcheva**[1], **Bipasha Mukherjee**[1], **Brian McEllin**[2], **Vamsidhara Vemireddy**[2], **Kimmo Hatanpaa**[3], **Michael D. Story**[1], **Amyn A. Habib**[2,4], **Vundavalli V. Murty**[5], **Robert Bachoo**[2], and **Sandeep Burma**[1,*]

[1]Department of Radiation Oncology, University of Texas Southwestern Medical Center, Dallas, TX

[2]Department of Neurology and Neurotherapeutics, University of Texas Southwestern Medical Center, Dallas, TX

[3]Department of Pathology, University of Texas Southwestern Medical Center, Dallas, TX

[4]VA North Texas Health Care System, Dallas, TX

[5]Department of Pathology and Cell Biology, Columbia University Medical Center, New York, NY

Abstract

Glioblastomas (GBM) are highly radioresistant and lethal brain tumors. Ionizing radiation (IR)-induced DNA double-strand breaks (DSBs) are a risk factor for the development of GBM. In this study, we systematically examined the contribution of IR-induced DSBs to GBM development using transgenic mouse models harboring brain-targeted deletions of key tumor suppressors frequently lost in GBM, namely *Ink4a*, *Ink4b*, *Arf*, and/or *PTEN*. Using low linear energy transfer (LET) X-rays to generate simple breaks or high LET Fe ions to generate complex breaks, we found that DSBs induce high-grade gliomas in these mice which, otherwise, do not develop gliomas spontaneously. Loss of *Ink4a* and *Arf* was sufficient to trigger IR-induced glioma development but additional loss of *Ink4b* significantly increased tumor incidence. We analyzed IR-induced tumors for copy number alterations (CNAs) to identify oncogenic changes that were generated and selected for as a consequence of stochastic DSB events. We found Met amplification to be the most significant oncogenic event in these radiation-induced gliomas. Importantly, Met activation resulted in expression of Sox2, a GBM cancer stem cell (CSC) marker, and was obligatory for tumor formation. In sum, these results indicate that radiation-

*Address correspondence to: Division of Molecular Radiation Biology, Department of Radiation Oncology, University of Texas Southwestern Medical Center, 2201 Inwood Road, NC7.214E, Dallas, Texas 75390, USA; Tel: 214-648-7440; Fax: 214-648-5995; sandeep.burma@utsouthwestern.edu.
[6]Current address: St. Jude Children's Research Hospital, Memphis, TN

induced DSBs cooperate with loss of Ink4 and Arf tumor suppressors to generate high-grade gliomas that are commonly driven by Met amplification and activation.

Keywords

Glioblastoma (GBM); Ionizing Radiation (IR); DNA double-strand break (DSB); Met; Ink4; Arf

Introduction

Glioblastoma (GBM) is the most common primary malignant brain tumor and is highly fatal despite aggressive treatment regimens that include surgical resection, radiotherapy, and chemotherapy (1-3). Following surgery, the residual tumor is commonly treated with cumulative radiation doses of 60 Gy or more. In spite of such aggressive treatment, tumor recurrence is quick and the relapsed tumor is highly therapy resistant. A clear understanding of factors contributing to glioblastoma development and recurrence is necessary for the formulation of effective therapeutic strategies. Exposure to ionizing radiation (IR) is the only known risk factor for developing these lethal brain tumors (4-9), and even low dose radiation exposure from CT scans has been reported to increase the risk of subsequent brain tumor development (10).

In order to directly examine the contribution of IR to GBM development, we intracranially irradiated a cohort of Nestin-Cre mice with brain-targeted deletions of *Ink4a*, *Ink4b*, *Arf*, and/or *PTEN*, tumor suppressor genes that are frequently lost in GBM (1-3). Two different types of IR, low linear energy transfer (LET) X-rays and high LET Fe ions, were used to induce simple and complex DNA double-strand breaks (DSBs), respectively (11-13). We found that exposure to IR precipitated the development of high-grade gliomas in these mice, with frequencies depending upon the combination of tumor suppressor gene deletion(s), as well as upon the radiation dose and quality. Strikingly, we found high levels of amplification of the Met receptor tyrosine kinase (RTK) to be the predominant genomic alteration in these IR-induced tumors. Interestingly, Met over-expression not only promoted tumorigenesis, but also conferred a stem cell phenotype via upregulation of Sox2 in these tumors.

Results and Discussion

Induction and repair of DNA double-strand breaks in the mouse brain

For this study, we used the following compound transgenic mouse lines in which GBM-relevant tumor suppressor genes are conditionally deleted in the brain: 1) Nestin-Cre;Ink4a/Arf$^{+/+}$ (designated WT for wild type), 2) Nestin-Cre;Ink4a/Arf$^{f/f}$ (designated Ink4a/Arf$^{-/-}$), 3) Nestin-Cre;Ink4ab$^{-/-}$;Arf$^{f/f}$ (designated Ink4ab/Arf$^{-/-}$), and 4) Nestin-Cre;Ink4ab$^{-/-}$;Arf$^{f/f}$;PTEN$^{f/+}$ (designated Ink4ab/Arf$^{-/-}$;PTEN$^{+/-}$) (Supplementary Table 1). We monitored the induction of DSBs, the most deleterious lesion inflicted by IR (14), in the brains of WT (Supplementary Figure S1a) and Ink4ab/Arf$^{-/-}$ (Figure 1a) mice that were intra-cranially irradiated with a single dose of 1 Gy Fe ions or 4 Gy X-rays (equitoxic doses based on the colony formation assay (15)). DSBs were quantified by counting γH2AX foci, a marker for DSBs, in brain sections at different times post-IR, as previously described (16).

DSBs were quantified in the two neurogenic niches, the subgranular zone (SGZ) and subventricular zone (SVZ) (17), as well as in the cortex and in astrocytes (GFAP-positive cells). At 1 hour post-IR, we observed the induction of DSBs in all regions of the WT and Ink4ab/Arf$^{-/-}$ mouse brains (Figure 1b and Supplementary Fig. 1b). By 12 hours post-IR, a high level of apoptosis (TUNEL positivity) was seen in the SVZ (Figure 1c and Supplementary Fig. 1c), along with a concomitant decrease in the number of proliferating (Ki67-positive) cells (Figure 1d and Supplementary Figure 1d), thus confirming the induction of DNA damage by both low and high LET IR. We found that DSBs induced by X-rays were rapidly repaired while those induced by Fe ions were persistent, as was evident from comparing residual breaks at 1 and 3 days post-IR (Figure 1b). Even at 1 month post-IR, approximately 13% of Fe-irradiated cells harbored at least one γH2AX focus (Supplementary Fig. 1b). WT and Ink4ab/Arf$^{-/-}$ brains displayed similar DNA repair capabilities indicating that deletions of Ink4a, Ink4b, and Arf tumor suppressors did not affect the repair of IR-induced DSBs *per se* (Figure 1b).

Combined inactivation of Ink4a, Ink4b, and Arf cooperates with IR-induced DSBs to generate high-grade gliomas

WT, Ink4a/Arf$^{-/-}$, Ink4ab/Arf$^{-/-}$, and Ink4ab/Arf$^{-/-}$;PTEN$^{+/-}$ mice, at 6-10 weeks of age, were irradiated intra-cranially with a single dose of 1 Gy Fe or with an equitoxic dose of 4 Gy X-rays (Supplementary Table 1). Unlike typical mouse GBM models (1, 18), these mice lack a dominantly-acting oncogene and thus do not develop brain lesions spontaneously, except for a small percentage of Ink4ab/Arf$^{-/-}$;PTEN$^{+/-}$ mice (Supplementary Table 1). Exposure to either X-rays or Fe ions resulted in brain tumors in mice with tumor suppressor gene deletions, but not in WT mice. Brain tumor incidence in Ink4ab/Arf$^{-/-}$ mice was higher than in Ink4a/Arf$^{-/-}$ mice (25% and 10%, respectively). Additional PTEN heterozygosity increased tumor incidence after Fe irradiation to 35% (Supplementary Table 1 and Figure 2a). Four-fold lower doses of Fe ions compared to X-rays (1 Gy *vs* 4 Gy) were needed to achieve similar tumor frequencies. Thus, Fe ions appear to have an approximately 4-fold higher relative biological effectiveness (RBE) for transformation compared to X-rays, very similar to the RBE for cell killing in colony formation assays (15). Taken together, these results clearly indicate that DSBs, both simple and complex, can cooperate with deletions of the *Ink4* and *Arf* genes to promote malignant transformation in the mouse brain.

All IR-induced tumors obtained were highly infiltrative, exhibiting markedly increased cellularity (Figure 2b), high mitotic activity, and pleomorphic nuclei, with areas of pseudopalisading necrosis (Figure 2c). These tumors were classified as high-grade glial tumors (Grade III or IV) after pathological examination, based on the World Health Organization classification system (1). Tumors from Ink4ab/Arf$^{-/-}$ mice (Figure 2d), as well as from other genotypes (Supplementary Figure 2), stained positive for Nestin, GFAP, NeuN and Olig2 to varying extents, all of which are classical human glioma markers (19). Tumors also showed elevated levels of phospho-Erk and phospho-Akt, indicating activation of Ras and Akt signaling pathways, respectively, and high numbers of Ki67-positive cells, indicating robust proliferation as seen in human GBM.

IR-induced glioblastomas are characterized by a high frequency and amplitude of Met amplification

In order to identify genomic changes driving IR-induced gliomagenesis, we analyzed Fe-induced tumors from Ink4ab/Arf$^{-/-}$ mice using array comparative genomic hybridization (aCGH) (Figure 3a). The data set was analyzed using the Genomic Identification of Significant Targets in Cancer (GISTIC) algorithm that identifies regions of copy number variation (CNV) that are more likely to drive cancer pathogenesis by emphasizing frequency of occurrence as well amplitude of the aberration (20). Upon analysis of 12 Ink4ab/Arf$^{-/-}$ tumors, we identified 76 genes with G scores >5 (Appendix). The most significant and frequent amplification (G score= 25.3), found present in ~42% (5/12) of tumors examined, localized to a small region on Chr6A2, where the RTK Met was the only gene spanned by the peak of the CNV (Figure 3a). The amplitude of Met amplification was high, with log2 ratios typically above 3, implying more than 8 gene copies per cell (Figure 3b). Other RTKs implicated in glioma development, namely PDGFRβ and EGFR (1), were found to be amplified in 16.6% (2/12) and 8.3% (1/12) of tumors, respectively. Log2 ratios for these two genes were between 0.5 and 1, indicating low copy number amplification (Supplementary Figure 3a). Met amplification was largely confirmed by fluorescence in situ hybridization (FISH) analyses of 8 tumors that had been previously analyzed by aCGH (Supplementary Table 2). Amplification was predominantly in the form of extra-chromosomal double minutes (Figure 3c) similar to that reported for human GBM (21). In most tumors examined by FISH, Met amplification was uniform, with every tumor cell showing evidence of amplification, indicating that this was an early event in gliomagenesis in these models similar to that postulated for human GBM (22). A limited number of tumors derived from other genotypes and radiation types were also analyzed by aCGH and/or FISH and frequent Met amplification was observed in these IR-induced tumors (Supplementary Figure 3b and Supplementary Table 2). Finally, amplification correlated with robust Met expression and activation as confirmed by immunohistochemical staining of representative tumors with anti-Met and anti-phospho-Met antibodies, respectively (Figure 3d).

Met amplification in IR-induced tumors correlates with Sox2 expression and promotes tumorigenesis

We established *ex vivo* cultures from tumors obtained from X-ray or Feirradiated Ink4ab/Arf$^{-/-}$ mice. However, even for tumors that were highly positive for Met, the derivative cultures showed barely detectable Met protein levels by Western blotting (Supplementary Figure 4a), indicating loss of Met double minutes due to absence of selection pressure under *in vitro* culture conditions. This phenomenon is similar to that reported for Met amplified in breast cancers (23), and is analogous to that seen with EGFR or EGFRvIII in human GBM cultures (24). We therefore re-expressed V5-tagged Met in a representative Fe-derived Ink4ab/Arf$^{-/-}$ tumor line (tumor ID#253). The Met re-expressing tumor line showed high levels of phosphorylated Met compared to control cells (parental tumor line expressing V5-tagged β-Gal) (Figure 4a). A recent report highlighted a potential role for Met in maintaining a GBM CSC-like phenotype via up regulation of Sox2, a re-programming transcription factor involved in the maintenance of neural stem cells (NSC) (25). We, too, found that re-expression of Met resulted in high levels of Sox2 expression (Figures 4a,b) and conferred an

ability to grow as neurospheres in serum-free NSC media (Figure 4c). Met expression also enhanced the ability of these cells to grow as colonies in soft agar indicating that these cells were highly transformed compared to the control cells (Figure 4d). Finally, to confirm the importance of Met in promoting tumorigenesis in our model system, we injected cells re-expressing Met subcutaneously into nude mice. As few as 20,000 Met-expressing cells were sufficient to generate palpable tumors by 8 weeks indicating that these cells were highly tumorigenic (Figure 4e). By comparison, even 2.5 million control cells were unable to generate palpable tumors within this time frame. In a complementary set of experiments, we generated a tumor cell line with high levels of Met expression by passaging an *ex vivo* culture as an allograft (Supplementary Figure 4a). These cells showed significantly enhanced Sox2 expression (Supplementary Figure 4b,c) and stem cell and tumorigenic phenotypes (Supplementary Figure 4d,e) compared to the parental cultures (which had low levels of Met), and this was reversed by shRNA-mediated knockdown of Met. Importantly, higher levels of Sox2 expression were also seen in the radiation-induced gliomas with Met amplification compared to non-amplified tumors (Figure 3d).Taken together, these results indicate that Met amplification is important both for enhancing tumorigenicity as well as for promoting Sox2 expression and a CSC phenotype in the context of radiation-induced gliomas in these model systems.

In this study, we directly examined the role of IR-induced DSBs, in cooperation with existing tumor suppressor losses, in the development of high-grade gliomas using genetically accurate mouse GBM models. The greatest advantage of this approach is that, without forced expression of a dominant oncogene, it allows for the selection of genetic alterations arising from stochastic events that may play a crucial role in gliomagenesis. Our "sensitized" models, with targeted deletions of *Ink4a, Ink4b,* and *Arf*, are very appropriate for this study given that these loci are commonly deleted in about 50% of GBMs (26) and loss of these loci is suggested to be one of the earliest initiating events in gliomagenesis (27). Our results indicate that combined loss of these three tumor suppressors (Ink4a, Ink4b, and Arf), while insufficient for gliomagenesis *per se*, cooperate with IR-induced DSBs to efficiently induce high-grade gliomas. We find that the frequency of tumor formation depends both upon the tumor suppressor gene deletion(s) as well as upon the radiation dose and quality. We used two qualitatively different types of IR for this study, X- rays and Fe particles. While X-rays are commonly used for therapy, particle radiation is also being increasingly used in the clinic due to better dose distribution and higher RBE (11-13). In addition, heavier particles, such as Fe ions, are a common component of Galactic Cosmic Rays (GCR) and pose a clear cancer risk to astronauts, the magnitude of which remains to be quantified. We found that lower doses of Fe ions, compared to X-rays, are needed to generate tumors with the same frequency indicating that Fe ions have a higher transforming potential compared to X-rays. The higher transforming potential of Fe ions correlates with the slower repair of DSBs induced by these ions *in vivo* which is in accord with *in vitro* observations reported by us previously (15, 28). The slower repair observed with Fe ions is presumably due to the induction of clustered DNA damage that is inherently more difficult to repair (12, 13, 29) and also due to the propensity for such damage to undergo DNA end resection and be repaired by the slower process of homologous recombination (30-32). With both X-rays and Fe ions, we observed a significantly lower incidence of gliomas with loss of

Ink4a and Arf, compared to loss of Ink4a, Ink4b, and Arf, corroborating both our previous *in vitro* study showing that additional loss of Ink4b accompanies IR-induced transformation of Ink4a/Arf-null astrocytes (15) and an independent study demonstrating that Ink4b plays an important "backup" tumor suppressor role in the absence of Ink4a (33). Additional heterozygous loss of PTEN increases the frequency of brain tumors after Fe irradiation, in accord with the role of PTEN loss in promoting gliomagenesis in humans (1-3). Taken together, our results indicate that DSBs, whether simple or complex (i.e., resulting from X-ray or Fe-irradiation), generate high-grade gliomas in these mouse models after exposure to an acute, clinically-relevant dose of IR, with Fe ions exhibiting at least a 4-fold higher transforming potential compared to X-rays.

Detailed analyses of the IR-induced tumors from Ink4ab/Arf$^{-/-}$ mice revealed that amplification of the RTK Met was strongly selected for during tumorigenesis and that Met expression conferred a high tumorigenic potential to the glioma cells. MET is frequently amplified or mutationally activated in many human cancers and triggers a diverse array of downstream signaling cascades that promote cell survival, growth, invasion, and metastasis of cancer cells (34, 35). Focal amplification of MET occurs in about 4% of human GBM (26). However, broad amplification of chromosome 7 (which harbors the *MET* gene) occurs in about 80% of primary GBM, and at least a third of chromosome 7 gain events are associated with overexpression of MET and/or its ligand HGF (20). A recent study mapping the evolution of glioblastomas in human patients identified MET amplification as an early event during gliomagenesis (22). Importantly, MET has recently been shown to be amplified and activated in GBM CSCs where it is involved in maintaining a stem cell-like phenotype by promoting the expression of re-programming transcription factors such as Nanog and Sox2 (25). A CSC-maintenance role for MET was bolstered by recent studies showing that MET amplification is a functional marker for GBM CSCs (36, 37). Our results, showing that Met promotes Sox2 expression and the ability of glioma cells to grow as neurospheres, support such a CSC-maintenance role for Met.

It has been reported that MET amplification in human tumors might be a consequence of DNA breakages occurring within chromosomal fragile sites (38); thus, it is conceivable that IR-induced DSBs might trigger MET amplification during radiotherapy of human GBM. Importantly, MET expression correlates with resistance to therapeutic agents (39-44) including IR (45). Thus, our results raise the possibility that recurrent tumors arising after radiotherapy might have a greater propensity for MET amplification, rendering them even more resistant to therapy compared to primary tumors. Indeed, in studies involving a limited number of matched pre- and post-irradiated (recurrent) tumor specimens, MET levels were found to be higher in recurrent tumors compared to the corresponding primary tumor; moreover, patients showing higher levels of MET induction after therapy had a significantly shorter median survival compared to patients with lower levels of MET induction (37, 46). A causal relationship between radiation and MET amplification may help explain why there is a lack of significant representation of GBMs showing concomitant over-expression of MET and Sox2 in the TCGA database where approximately 90% of the GBM specimens are primary tumors that did not receive radiotherapy (26). Our results, for the first time, demonstrate the process of radiation-induced gliomagenesis in genetically-defined mouse

GBM models and raise the possibility that Met amplification may drive glioblastoma development or recurrence upon exposure to IR. Taken together, these results have important implications not just for IR-induced gliomagenesis but also for the development of therapy-resistant recurrent tumors that arise after GBM radiotherapy.

Supplementary Material

Refer to Web version on PubMed Central for supplementary material.

Acknowledgements

References

1. Furnari FB, Fenton T, Bachoo RM, Mukasa A, Stommel JM, Stegh A, et al. Malignant astrocytic glioma: genetics, biology, and paths to treatment. Genes Dev. Nov 1; 2007 21(21):2683–710. [PubMed: 17974913]

2. Westphal M, Lamszus K. The neurobiology of gliomas: from cell biology to the development of therapeutic approaches. Nat Rev Neurosci. Sep; 2011 12(9):495–508. [PubMed: 21811295]

3. Purow B, Schiff D. Advances in the genetics of glioblastoma: are we reaching critical mass? Nat Rev Neurol. Aug; 2009 5(8):419–26. [PubMed: 19597514]

4. Bondy ML, Scheurer ME, Malmer B, Barnholtz-Sloan JS, Davis FG, Il'yasova D, et al. Brain tumor epidemiology: consensus from the Brain Tumor Epidemiology Consortium. Cancer. Oct 1; 2008 113(7 Suppl):1953–68. [PubMed: 18798534]

5. Ron E. Ionizing radiation and cancer risk: evidence from epidemiology. Pediatr Radiol. Apr; 2002 32(4):232–7. discussion 42-4. [PubMed: 11956701]

6. Neglia JP, Meadows AT, Robison LL, Kim TH, Newton WA, Ruymann FB, et al. Second neoplasms after acute lymphoblastic leukemia in childhood. N Engl J Med. Nov 7; 1991 325(19): 1330–6. [PubMed: 1922234]

7. Salvati M, Frati A, Russo N, Caroli E, Polli FM, Minniti G, et al. Radiation-induced gliomas: report of 10 cases and review of the literature. Surg Neurol. Jul; 2003 60(1):60–7. discussion 7. [PubMed: 12865017]

8. Thierry-Chef I, Simon SL, Land CE, Miller DL. Radiation dose to the brain and subsequent risk of developing brain tumors in pediatric patients undergoing interventional neuroradiology procedures. Radiat Res. Nov; 2008 170(5):553–65. [PubMed: 18959462]

9. Paulino AC, Mai WY, Chintagumpala M, Taher A, Teh BS. Radiation-induced malignant gliomas: is there a role for reirradiation? Int J Radiat Oncol Biol Phys. Aug 1; 2008 71(5):1381–7. [PubMed: 18262733]

10. Pearce MS, Salotti JA, Little MP, McHugh K, Lee C, Kim KP, et al. Radiation exposure from CT scans in childhood and subsequent risk of leukaemia and brain tumours: a retrospective cohort study. Lancet. Aug 4; 2012 380(9840):499–505. [PubMed: 22681860]

11. Durante M, Cucinotta FA. Heavy ion carcinogenesis and human space exploration. Nat Rev Cancer. Jun; 2008 8(6):465–72. [PubMed: 18451812]

12. Okayasu R. Repair of DNA damage induced by accelerated heavy ions--a mini review. Int J Cancer. Mar 1; 2012 130(5):991–1000. [PubMed: 21935920]

13. Sage E, Harrison L. Clustered DNA lesion repair in eukaryotes: relevance to mutagenesis and cell survival. Mutat Res. Jun 3; 2011 711(1-2):123–33. [PubMed: 21185841]

14. Khanna KK, Jackson SP. DNA double-strand breaks: signaling, repair and the cancer connection. Nat Genet. Mar; 2001 27(3):247–54. [PubMed: 11242102]

15. Camacho CV, Mukherjee B, McEllin B, Ding LH, Hu B, Habib AA, et al. Loss of p15/Ink4b accompanies tumorigenesis triggered by complex DNA double-strand breaks. Carcinogenesis. Oct; 2010 31(10):1889–96. [PubMed: 20663777]

16. Mukherjee B, McEllin B, Camacho CV, Tomimatsu N, Sirasanagandala S, Nannepaga S, et al. EGFRvIII and DNA double-strand break repair: a molecular mechanism for radioresistance in glioblastoma. Cancer Res. May 15; 2009 69(10):4252–9. [PubMed: 19435898]

17. Sutter R, Yadirgi G, Marino S. Neural stem cells, tumour stem cells and brain tumours: dangerous relationships? Biochim Biophys Acta. Dec; 2007 1776(2):125–37. [PubMed: 17868999]

18. Hambardzumyan D, Parada LF, Holland EC, Charest A. Genetic modeling of gliomas in mice: new tools to tackle old problems. Glia. Aug; 2011 59(8):1155–68. [PubMed: 21305617]

19. Louis DN, Ohgaki H, Wiestler OD, Cavenee WK, Burger PC, Jouvet A, et al. The 2007 WHO classification of tumours of the central nervous system. Acta Neuropathol. Aug; 2007 114(2):97–109. [PubMed: 17618441]

20. Beroukhim R, Getz G, Nghiemphu L, Barretina J, Hsueh T, Linhart D, et al. Assessing the significance of chromosomal aberrations in cancer: methodology and application to glioma. Proc Natl Acad Sci U S A. Dec 11; 2007 104(50):20007–12. [PubMed: 18077431]

21. Fischer U, Muller HW, Sattler HP, Feiden K, Zang KD, Meese E. Amplification of the MET gene in glioma. Genes Chromosomes Cancer. Jan; 1995 12(1):63–5. [PubMed: 7534113]

22. Sottoriva A, Spiteri I, Piccirillo SG, Touloumis A, Collins VP, Marioni JC, et al. Intratumor heterogeneity in human glioblastoma reflects cancer evolutionary dynamics. Proc Natl Acad Sci U S A. Mar 5; 2013 110(10):4009–14. [PubMed: 23412337]

23. Smolen GA, Muir B, Mohapatra G, Barmettler A, Kim WJ, Rivera MN, et al. Frequent met oncogene amplification in a Brca1/Trp53 mouse model of mammary tumorigenesis. Cancer Res. Apr 1; 2006 66(7):3452–5. [PubMed: 16585167]

24. Bigner SH, Humphrey PA, Wong AJ, Vogelstein B, Mark J, Friedman HS, et al. Characterization of the epidermal growth factor receptor in human glioma cell lines and xenografts. Cancer Res. Dec 15; 1990 50(24):8017–22. [PubMed: 2253244]

25. Li Y, Li A, Glas M, Lal B, Ying M, Sang Y, et al. c-Met signaling induces a reprogramming network and supports the glioblastoma stem-like phenotype. Proc Natl Acad Sci U S A. Jun 14; 2011 108(24):9951–6. [PubMed: 21628563]

26. McLendon R, Friedman A, Bigner D, Van Meir EG, Brat DJ, Mastrogianakis M, et al. Comprehensive genomic characterization defines human glioblastoma genes and core pathways. Nature. Sep 4.2008

27. Attolini CS, Cheng YK, Beroukhim R, Getz G, Abdel-Wahab O, Levine RL, et al. A mathematical framework to determine the temporal sequence of somatic genetic events in cancer. Proc Natl Acad Sci U S A. Oct 12; 2010 107(41):17604–9. [PubMed: 20864632]

28. Mukherjee B, Camacho CV, Tomimatsu N, Miller J, Burma S. Modulation of the DNA-damage response to HZE particles by shielding. DNA Repair (Amst). Oct 1; 2008 7(10):1717–30. [PubMed: 18672098]

29. Costes SV, Boissiere A, Ravani S, Romano R, Parvin B, Barcellos-Hoff MH. Imaging features that discriminate between foci induced by high- and low-LET radiation in human fibroblasts. Radiat Res. May; 2006 165(5):505–15. [PubMed: 16669704]

30. Saha J, Wang M, Cucinotta FA. Investigation of switch from ATM to ATR signaling at the sites of DNA damage induced by low and high LET radiation. DNA Repair (Amst). Dec; 2013 12(12):1143–51. [PubMed: 24238855]

31. Wang H, Wang X, Zhang P, Wang Y. The Ku-dependent non-homologous end-joining but not other repair pathway is inhibited by high linear energy transfer ionizing radiation. DNA Repair (Amst). May 3; 2008 7(5):725–33. [PubMed: 18325854]

32. Yajima H, Fujisawa H, Nakajima NI, Hirakawa H, Jeggo PA, Okayasu R, et al. The complexity of DNA double strand breaks is a critical factor enhancing end-resection. DNA Repair (Amst). Nov; 2013 12(11):936–46. [PubMed: 24041488]

33. Krimpenfort P, Ijpenberg A, Song JY, van der Valk M, Nawijn M, Zevenhoven J, et al. p15Ink4b is a critical tumour suppressor in the absence of p16Ink4a. Nature. Aug 23; 2007 448(7156):943–6. [PubMed: 17713536]

34. Trusolino L, Bertotti A, Comoglio PM. MET signalling: principles and functions in development, organ regeneration and cancer. Nat Rev Mol Cell Biol. Dec; 2010 11(12):834–48. [PubMed: 21102609]

35. Gherardi E, Birchmeier W, Birchmeier C, Vande Woude G. Targeting MET in cancer: rationale and progress. Nat Rev Cancer. Feb; 2012 12(2):89–103. [PubMed: 22270953]

36. De Bacco F, Casanova E, Medico E, Pellegatta S, Orzan F, Albano R, et al. The MET Oncogene Is a Functional Marker of a Glioblastoma Stem Cell Subtype. Cancer Res. Sep 1; 2012 72(17):4537–50. [PubMed: 22738909]

37. Joo KM, Jin J, Kim E, Ho Kim K, Kim Y, Gu Kang B, et al. MET Signaling Regulates Glioblastoma Stem Cells. Cancer Res. Aug 1; 2012 72(15):3828–38. [PubMed: 22617325]

38. Hellman A, Zlotorynski E, Scherer SW, Cheung J, Vincent JB, Smith DI, et al. A role for common fragile site induction in amplification of human oncogenes. Cancer Cell. Feb; 2002 1(1):89–97. [PubMed: 12086891]

39. Li Y, Lal B, Kwon S, Fan X, Saldanha U, Reznik TE, et al. The scatter factor/hepatocyte growth factor: c-met pathway in human embryonal central nervous system tumor malignancy. Cancer Res. Oct 15; 2005 65(20):9355–62. [PubMed: 16230398]

40. Laterra J, Rosen E, Nam M, Ranganathan S, Fielding K, Johnston P. Scatter factor/hepatocyte growth factor expression enhances human glioblastoma tumorigenicity and growth. Biochem Biophys Res Commun. Jun 27; 1997 235(3):743–7. [PubMed: 9207232]

41. Engelman JA, Zejnullahu K, Mitsudomi T, Song Y, Hyland C, Park JO, et al. MET amplification leads to gefitinib resistance in lung cancer by activating ERBB3 signaling. Science. May 18; 2007 316(5827):1039–43. [PubMed: 17463250]

42. Jun HJ, Acquaviva J, Chi D, Lessard J, Zhu H, Woolfenden S, et al. Acquired MET expression confers resistance to EGFR inhibition in a mouse model of glioblastoma multiforme. Oncogene. Jun 21; 2012 31(25):3039–50. [PubMed: 22020333]

43. Turke AB, Zejnullahu K, Wu YL, Song Y, Dias-Santagata D, Lifshits E, et al. Preexistence and clonal selection of MET amplification in EGFR mutant NSCLC. Cancer Cell. Jan 19; 2010 17(1):77–88. [PubMed: 20129249]

44. Stommel JM, Kimmelman AC, Ying H, Nabioullin R, Ponugoti AH, Wiedemeyer R, et al. Coactivation of receptor tyrosine kinases affects the response of tumor cells to targeted therapies. Science. Oct 12; 2007 318(5848):287–90. [PubMed: 17872411]

45. De Bacco F, Luraghi P, Medico E, Reato G, Girolami F, Perera T, et al. Induction of MET by ionizing radiation and its role in radioresistance and invasive growth of cancer. J Natl Cancer Inst. Apr 20; 2011 103(8):645–61. [PubMed: 21464397]

46. Liu W, Fu Y, Xu S, Ding F, Zhao G, Zhang K, et al. c-Met expression is associated with time to recurrence in patients with glioblastoma multiforme. J Clin Neurosci. Jan; 2011 18(1):119–21. [PubMed: 20832323]

47. Isaka F, Ishibashi M, Taki W, Hashimoto N, Nakanishi S, Kageyama R. Ectopic expression of the bHLH gene Math1 disturbs neural development. Eur J Neurosci. Jul; 1999 11(7):2582–8. [PubMed: 10383648]

48. Krimpenfort P, Quon KC, Mooi WJ, Loonstra A, Berns A. Loss of p16Ink4a confers susceptibility to metastatic melanoma in mice. Nature. Sep 6; 2001 413(6851):83–6. [PubMed: 11544530]

49. Podsypanina K, Ellenson LH, Nemes A, Gu J, Tamura M, Yamada KM, et al. Mutation of Pten/ Mmac1 in mice causes neoplasia in multiple organ systems. Proc Natl Acad Sci U S A. Feb 16; 1999 96(4):1563–8. [PubMed: 9990064]

50. Scotto L, Narayan G, Nandula SV, Subramaniyam S, Kaufmann AM, Wright JD, et al. Integrative genomics analysis of chromosome 5p gain in cervical cancer reveals target over-expressed genes, including Drosha. Mol Cancer. 2008; 7:58. [PubMed: 18559093]
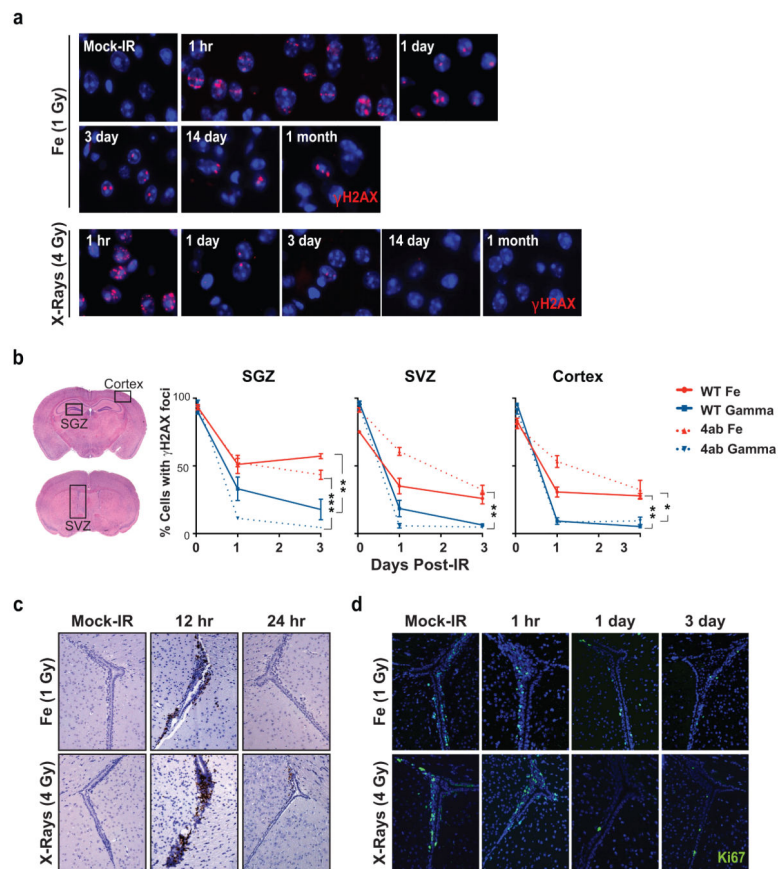
Figure 1. Induction and repair of DSBs in the mouse brain

(a) Ink4ab/Arf $^{-/-}$ mice were irradiated intra-cranially with 1 Gy of Fe ions or 4 Gy of X-rays and DNA damage examined at the indicated time points. Fe ions with a kinetic energy of 600 MeV/nucleon were provided by the National Aeronautics and Space Administration (NASA) Space Radiation Laboratory at Brookhaven National Laboratory, as described previously (28). X-ray irradiations were carried out using an X-RAD 320 irradiator (Precision X-Ray). DNA damage was visualized by staining for γH2AX (red, Millipore, Billerica, MA); nuclei were stained with DAPI (blue). Immunofluorescence staining of tissue sections was performed as described previously (16). Representative pictures of the cortical region are shown. Mice were obtained from the Mouse Cancer Models Consortium and maintained in a FVB/NJ and C57BL6 mixed background. Nestin-Cre mice (47) were crossed with two previously described transgenic mouse lines, Ink4a/Arf $^{f/f}$ harboring floxed *Ink4a* and *Arf* genes (48) or Ink4ab$^{-/-}$;Arf $^{f/f}$, harboring germline inactivation of *Ink4a* and *Ink4b*, and a floxed *Arf* gene (33). Additional PTEN heterozygosity (PTEN$^{f/+}$) (49) was bred into the Ink4ab$^{-/-}$;Arf$^{f/f}$ background. All procedures for mouse experiments were performed under protocols approved by the Institutional Animal Care and Use Committees of the University of Texas Southwestern Medical Center and the Brookhaven National Laboratory. (b) DNA damage was quantified in the SGZ, SVZ, and cortex by calculating the percentage of nuclei with at least 1 γH2AX focus (y-axis) at the indicated times post-IR (x-axis). Initial damage was measured at 1 hour post-IR and mice were monitored up to 1 month post-IR. γH2AX data (1 to72 hours post-IR) for WT (Supplementary Figure S1a) and Ink4ab/Arf $^{-/-}$

mice are plotted together to allow direct comparisons; data for the entire one-month time course are shown in Supplementary Figure S1b. Note higher percentage of cells with γH2AX foci in Fe-irradiated brains at 3 days post-IR and no major difference in repair capacity between WT and Ink4ab/Arf $^{-/-}$ mice. n = 3 mice per time point. Error bars, S.E.M. p-values for X-rays *vs* Fe ions are: **, p = 0.0072 (SGZ of WT mice); ***, p = 0.0003 (SGZ of Ink4ab/Arf$^{-/-}$ mice); **, p = 0.0085 (SVZ of WT mice); **, p = 0.0013 (SVZ of Ink4ab/Arf$^{-/-}$ mice); **, p = 0.0025 (cortex of WT mice); *, p = 0.0371 (cortex of Ink4ab/Arf$^{-/-}$ mice). Statistical significance was calculated by performing unpaired, two tailed t-tests using the Graphpad Prism software package. **(c)** Terminal deoxyribonucleotidyl transferase-mediated dUTP nick end labeling (TUNEL) staining was performed on brain sections of Ink4ab/Arf $^{-/-}$ and WT (Supplementary Figure S1c) mice at 12 and 24 hours post-IR. Note large numbers of apoptotic cells in the SVZ at 12 hours in response to both Fe- and X-ray irradiation. TUNEL assay was performed according to the manufacturer's instructions using FragEL DNA Fragmentation Kit with colorimetric TdT-Enzyme (Calbiochem, Darmstadt, Germany) to detect fragmentation of DNA associated with apoptosis on formalin-fixed paraffin embedded tissue sections. **(d)** Proliferating cells in the SVZ of Ink4ab/Arf $^{-/-}$ and WT (Supplementary Figure S1d) mice were visualized by staining with anti-Ki67 antibody (green; Novocastra, Wetzlar, Germany). Note loss of Ki67-positive cells after irradiation.
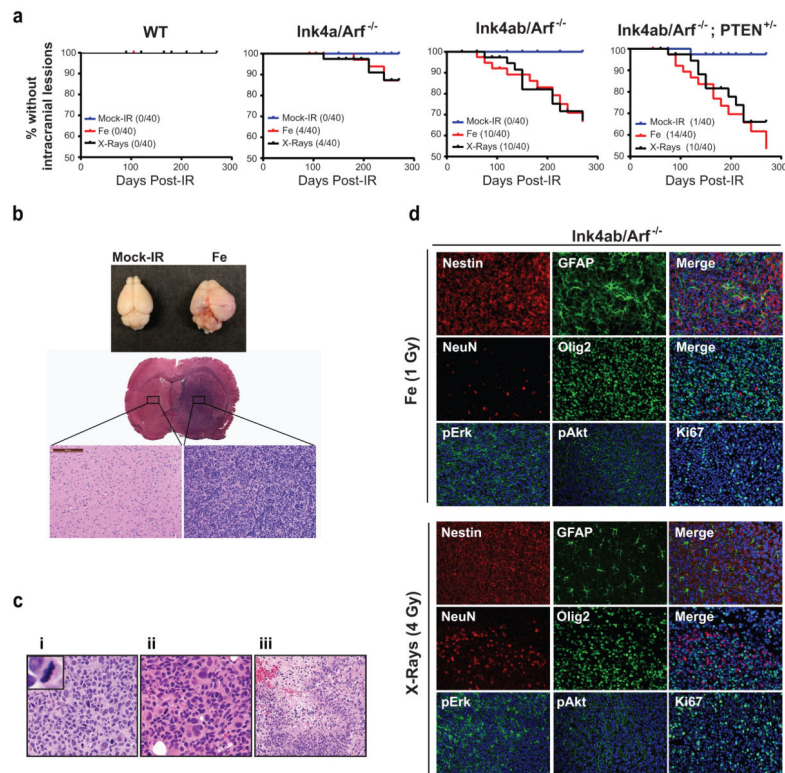
Figure 2. DSBs cooperate with tumor suppressor gene loss to generate high-grade gliomas
(a) Kaplan-Meier curves showing percentages of Fe- or X-ray-irradiated mice surviving without intracranial lesions for the four different genetic backgrounds. n = 40 mice per group (numbers in parentheses indicate total number of glioblastomas observed in each cohort). Note higher incidence of tumor formation in Ink4ab/Arf$^{-/-}$ cohort compared to Ink4a/Arf$^{-/-}$ cohort. p = 0.0270 (Mock-IR *vs* X-rays or Fe for Ink4a/Arf$^{-/-}$ mice); p = 0.0003 (Mock-IR *vs* X-rays or Fe for Ink4ab/Arf$^{-/-}$ mice); p = 0.0013 (Mock-IR *vs* X-rays for Ink4ab/Arf$^{-/-}$;PTEN$^{+/-}$ mice); p < 0.0001 (Mock-IR *vs* Fe for Ink4ab/Arf$^{-/-}$;PTEN$^{+/-}$ mice). Statistical significance was calculated by the logrank test using the Graphpad Prism software package. Mice were monitored for up to 9 months post-IR for onset of neurological symptoms (seizure, ataxia, lack of clasp reflex, or lack of balance) and for additional symptoms such as lethargy or weight loss. Mice exhibiting these symptoms or morbidity were sacrificed and examined for evidence of brain tumors by serial sectioning and Hematoxylin and Eosin (H&E) staining. Tumor classifications were assigned by a resident neuropathologist. To rule out occult lesions, all brains from asymptomatic mice were similarly screened at end of the experimental period. **(b)** Representative image of a tumor-bearing Ink4ab/Arf$^{-/-}$ brain at 2 months post-IR compared to a normal mock-irradiated brain and Hematoxylin and Eosin (H&E)-stained section of a representative Ink4ab/Arf$^{-/-}$ brain harboring a glioma. Note infiltrative nature and hypercellularity of the lesion. **(c)** Tumors were classified as high-grade gliomas based on a range of histopathological features including – (i) high mitotic activity (inset shows magnified view of a mitotic nucleus), (ii) pleomorphic nuclei, and (iii) areas with pseudopalisading necrosis. **(d)** Immunofluorescence staining of Ink4ab/Arf$^{-/-}$ tumors for classical human glioma markers, Nestin (BD

Pharmingen, San Diego, CA), GFAP (Biocare Medical, Concord, CA), NeuN (Millipore, Billerica, MA), and Olig2 (Millipore, Billerica, MA) was carried out as described previously (16). Tumors were also stained for phospho-Erk1/Erk2 (Thr202/Tyr204) (Abcam, Cambridge, MA), phospho-Akt (Ser473) (Abcam, Cambridge, MA), and Ki67 (Novocastra, Wetzlar, Germany).
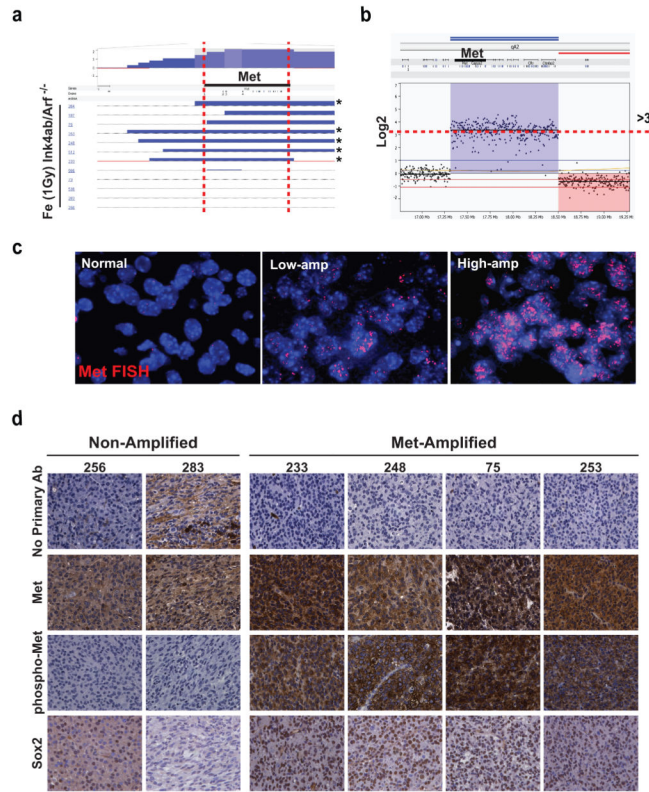
Figure 3. High frequency and amplitude of Met amplification in radiation-induced gliomas
(a) aCGH schematic of Met locus showing region of amplification (blue lines) across 12 Fe-derived tumor samples from Ink4ab/Arf$^{-/-}$ mice. Asterisks (*) indicate samples where region of amplification spanned the entire length of the Met locus. DNA was isolated from frozen tissues using the DNeasy Blood and Tissue Kit (Qiagen, Germantown, MD), following manufacturer's protocol. aCGH was carried out as previously described (15) and data analyzed using Nexus Copy Number Analysis software (Biodiscovery, El Segundo, CA). To identify meaningful copy number variation (CNV) events, the Genomic Identification of Significant Targets in Cancer (GISTIC) algorithm was used (20). This method calculates a statistic (G score) that takes into account frequency of the occurrence as well as amplitude of the aberration, and also calculates statistical significance for each aberration. By this method, Met amplification (G score= 25.3) was identified to be the most significant genomic alteration in these tumors. n = 12. **(b)** Representative probe view of chromosomal region flanking the Met locus showing log2 ratios (y-axis) of individual probes along the chromosome (x-axis). **(c)** FISH analysis showing representative radiation-induced tumors with normal, low, and high amplification levels of Met (red). A bacterial artificial chromosome (BAC) clone RP23-73G15 spanning the mouse Met gene was obtained from Invitrogen (Carlsbad, CA). DNA isolated from the BAC clone was labeled with Spectrum Orange dUTP by nick translation and used in FISH. FISH was performed on 4 μm sections prepared from formalin-fixed paraffin-embedded tissues using standard hybridization methods (50). Hybridization signals were analyzed on DAPI counterstained slides using a Nikon Eclipse epi-fluorescence microscope equipped with Applied Imaging CytoVision software (San Jose, CA). FISH signal scoring on tissue sections was restricted to

tumor areas based on H&E sections. **(d)** Immunohistochemical staining of 4 representative Met amplified tumors compared to 2 non-amplified tumors from Fe-irradiated Ink4ab/Arf$^{-/-}$ mice. Amplification of Met correlates with higher Met expression, robust activation of Met (phospho-Met), and increased levels of Sox2 expression. IHC was carried out using ImmPRESS peroxidaseconjugated secondary antibodies and the ImmPACT DAB peroxidase substrate (Vector Laboratories, Burlingame, CA), as specified by manufacturer. Antibodies used for IHC were anti-phospho-Met (Tyr1234/1235), anti-Met (Cell Signaling, Danvers, MA), and anti-Sox2 (Abcam, Cambridge, MA).

Figure 4. Met expression is associated with induction of Sox2 expression and high tumorigenic potential

(a) Western analysis of a representative Fe-derived tumor line (parental tumor ID#253), deficient in Ink4a, Ink4b, and Arf, and ectopically expressing V5-tagged Met or β-Gal as control. Primary astrocytes from WT and Ink4ab/Arf$^{-/-}$ mice serve as positive and negative Western blotting controls, respectively. Note that overexpression and activation of Met correlates with induction of high levels of Sox2. *Ex vivo* tumor cultures were all maintained in Dulbecco's Modified Eagle Medium (DMEM) containing 10% of a fetal bovine/newborn calf serum mixture and penicillin/streptomycin (50 mg/ml). To generate Met-expressing tumor cells, Met was sequentially cloned into pLenti6.3/V5-DEST vector using the Gateway Cloning system (Invitrogen, Carlsbad, CA) with pBabe-puro c-Met-WT as the starting vector (gift from Joan Brugge; Addgene, Cambridge, MA; plasmid #17493). Virus production was carried out using ViraPower Lentiviral Packaging Mix (Invitrogen, Carlsbad, CA), as specified by manufacturer. Cells were infected with viral particles at a multiplicity of infection (MOI) of 2 with 4μg/ml polybrene. Cells were maintained under selection with 4μg/ml blasticidin. Western blotting of whole-cell extracts was performed as described before (16). Antibodies used were anti-actin (Sigma, St Louis, MO), anti-phospho-Met (Tyr1234/1235), anti-Met, anti-Ink4b (Cell Signaling, Danvers, MA), anti-Sox2 (Abcam, Cambridge, MA), anti-Ink4a, anti-Arf (Santa Cruz, Dallas, TX), and anti-V5

(Invitrogen, Carlsbad, CA). **(b)** Immunofluorescence staining of Met-expressing and control cells showing correlation of Met expression (red) with Sox2 (green) was carried out as described previously (16). Antibodies used were anti-Met (Cell Signaling, Danvers, MA) and anti-Sox2 (Abcam, Cambridge, MA). **(c)** Bright field images of cells expressing β-Gal or Met growing as adherent cells in full serum, or as spheres in NSC media. Cells were plated in NSC media at single cell dilutions in 96-well plates to assay for sphere-formation. The percentage of cells forming neurospheres is plotted. n = 2. Note that control cells (expressing β-Gal) show no growth in NSC medium. NSC medium consisted of DMEM/ Ham's F12 50/50 mix with EGF (20ug/ml), bFGF (25ug/ml), progesterone (20ug/ml), B-27 and insulin/transferrin-selenium supplements, doxycycline (2mg/ml), penicillin/ streptomycin (50 mg/ml) and Fungizone antimycotic. **(d)** Tumorigenic potential of cells was assessed by colony formation in soft-agar. 1×10^4 cells were plated in 0.6% Bacto-agar. The percentage of cells forming colonies is plotted.n = 2. Error bars, S.E.M. ***, p = 0.009. Statistical significance was calculated by performing unpaired, two tailed t-tests using the Graphpad Prism software package. **(e)** Representative image of tumor resulting from sub-cutaneous injection of cells expressing Met at approximately 50 days post-injection. Note absence of tumor formation by control cells (expressing β-Gal). Cells (as indicated) were suspended in Hank's Buffered Salt Solution and 2×10^4, 1×10^5, 5×10^5, or 2.5×10^6 cells were subcutaneously injected into the flanks of 6-week-old Nu/Nu nude mice (Charles River Laboratories International, Wilmington, MA). Mice were monitored daily to determine days to palpability. Tumor development after injection of increasing numbers of Met-expressing (triangles) or control cells (crosses) is plotted. Plot shows the number of cells injected (x-axis) *versus* days until the resulting tumor became palpable (y-axis). Top section of plot shows injections that failed to form tumors up to 8 weeks. Note that 2×10^4 Met-expressing cells were sufficient to form tumors while even 2.5×10^6 control cells failed to form tumors within 8 weeks.